Adaptive Control of Electrostatic Microactuators With Bidirectional Drive

Keng Peng Tee, *Member, IEEE*, Shuzhi Sam Ge, *Fellow, IEEE*, and Francis Eng Hock Tay

***Abstract*—In this paper, adaptive control is presented for a class of single-degree-of-freedom (1DOF) electrostatic microactuator systems which can be actively driven bidirectionally. The control objective is to track a reference trajectory within the air gap without knowledge of the plant parameters. Both full-state feedback and output feedback schemes are developed, the latter being motivated by practical difficulties in measuring velocity of the moving plate. For the full-state feedback scheme, the system is transformed to the parametric strict feedback form, for which adaptive backstepping is performed to achieve asymptotic output tracking. Analogously, the output feedback design involved transformation to the parametric output feedback form, followed by the use of adaptive observer backstepping to achieve asymptotic output tracking. To prevent contact between the movable and fixed electrodes, special barrier functions are employed in Lyapunov synthesis. All closed-loop signals are ensured to be bounded. Extensive simulation studies illustrate the performance of the proposed control.**

***Index Terms*—Adaptive control, electrostatic devices, microactuators, nonlinear systems, observers.**

I. Introduction

THE advent of microelectromechanical systems (MEMs) technology, which allows for micro-scale devices to be batch-produced and processed at low costs, has ignited interest in the ways to control these devices effectively to enhance precision and speed of response. Electrostatic microactuators are widely employed in MEMs applications, due to simplicity of structure, ease of fabrication, and favorable scaling of electrostatic forces into the micro domain.

One of the main problems associated with unidirectional electrostatic actuation with open loop voltage control is the pull-in instability, a saddle node bifurcation phenomenon wherein the movable electrode snaps through to the fixed electrode once its displacement exceeds a fraction of the full gap. This places a severe limit on the operating range of electrostatic actuators. To overcome this problem, several methods have been reported. Closed-loop voltage control with position feedback was proposed to stabilize any point in the gap [1]. An alternative approach, which involved the passive addition of series capacitor, was found to extend the range of travel without any active feedback control circuitry [2], [3]. Charge feedback control design was employed to stabilize the dynamics of the electrical subsystem, which leads to the stabilization of entire system due to its minimum phase property [4], [5]. More advanced nonlinear control techniques were investigated in [6], including flatness-based control, Control Lyapunov function (CLF) synthesis, and backstepping control. In another study, different static and dynamic output feedback control were investigated and compared, including input-output linearization, linear state feedback, feedback passivation, and charge feedback schemes [7]. Furthermore, generalization of the static and dynamic output feedback control design to multi-degrees-of-freedom (DOFs) MEMs was proposed under a geometric framework [8].

Electrostatic micro-actuators with bidirectional drive are less prone to pull-in instability due to the fact that they can be actively controlled in both directions, unlike unidirectional drive actuators where only passive restoring force is provided by mechanical stiffness in one direction. The study of micro-actuators with bidirectional drive is important since its controllability is an advantage in high performance applications. For bidirectional parallel plate actuators, open loop control schemes based on oscillatory switching input were proposed to overcome pull-in instability and extend operation range [9], [10]. For bidirectional electrostatic comb actuators, a recent work compared the advantages and disadvantages between simple open- and closed-loop control strategies [11].

In most works on MEMs control, knowledge of model parameters is required and typically estimated through offline system identification methods. However, inconsistencies in bulk micromachining result in variation of parameters across devices, and may require extensive efforts in parameter identification, with higher costs. Furthermore, some of the parameters, such as the damping constant, are usually difficult to identify accurately, so a viable alternative is to rely on intelligent feedback control for online compensation of parametric uncertainties.

Recent years have witnessed the advent of intelligent control for nonlinear systems, which includes adaptive control and approximation-based control, among others. Adaptive control has been successful in handling not only linear plants, but also nonlinear plants with known structures but uncertain constant parameters (see, e.g., [12] and [13]). Furthermore, robustification techniques have been integrated with adaptive control to yield robustness properties with respect to unmodeled disturbances [14]. The marriage of adaptive control and backstepping yields a means of applying adaptive control to systems with

Manuscript received June 29, 2006; revised July 30, 2007. Manuscript received in final form April 17, 2008. First published November 25, 2008; current version published February 25, 2009. Recommended by Associate Editor K. Turner. This work was supported in part by A*Star SERC under Grant 052-101-0097.

K. P. Tee is with the Institute for Infocomm Research, Singapore 138632 (e-mail: kptee@i2r.a-star.edu.sg).

S. S. Ge is with the Social Robotics Lab, Interactive Digital Media Institute and the Department of Electrical and Computer Engineering, National University of Singapore, Singapore 117576 (e-mail: samge@nus.edu.sg).

F. E. H. Tay is with the Department of Mechanical Engineering, National University of Singapore, Singapore 117576 (e-mail: mpetayeh@nus.edu.sg).

Digital Object Identifier 10.1109/TCST.2008.2000981

non-matching conditions. The backstepping technique provides a systematic, recursive control design methodology that removes the restrictions of matching conditions [15], extended matching conditions [16], and growth conditions [17]. As a result, adaptive backstepping can be applied to a large class of nonlinear systems in parametric strict feedback form or pure feedback form. For the class of systems in parametric output feedback form, adaptive observer backstepping can be employed for stable control design, based on feedback of the output only [18].

There has been relatively few works in the literature on application of adaptive techniques in MEMs. Adaptive control was implemented in MEMs gyroscopes to compensate for non-ideal coupling effects between the vibratory modes [19]–[21]. In [22], by utilizing position, velocity, and acceleration information, adaptive parameter estimation was performed online and the parameter estimates fed into the inverse model of the system nonlinearities.

Motivated by our previous works on intelligent control for general nonlinear systems [23] and robotic manipulators [24], we apply adaptive backstepping control for single-DOF (1DOF) electrostatic microactuators with bidirectional drive, based on rigorous Lyapunov synthesis, to force the movable plate to track a reference trajectory within the air gap without knowledge of plant parameters. An early version of this work tackled the full-state feedback control design problem for a linear plant model [25]. In this paper, we provide a comprehensive treatment of both full-state and output feedback problems with respect to a nonlinear plant model that incorporates squeeze film damping effects. When full-state information is available, adaptive backstepping is carried out following a suitable change of coordinates that transform the system into parametric strict feedback form. When velocity feedback is unavailable, the plant is transformed into the parametric output feedback form and adaptive observer backstepping is employed to achieve asymptotic tracking without velocity measurement. Inspired by [26], we employ novel asymmetrical barrier functions in Lyapunov synthesis so as to design a control ensuring that the movable plate and the fixed electrodes do not come into contact. To the best of the authors' knowledge, the latter objective has not been tackled rigorously in published works on control of electrostatic microactuators, which usually base the control design on the unconstrained system and subsequently demonstrate by simulations that the constraints were not violated.

II. Problem Formulation and Preliminaries

Consider the dynamic model of the 1DOF electrostatic microactuator with bidirectional drive, as illustrated in Fig. 1. The capacitances C_f and C_b, between the movable plate and the top and bottom electrodes, respectively, are described by

$$C_f = \frac{\epsilon A}{l_0 - l} \quad C_b = \frac{\epsilon A}{l_0 + l} \tag{1}$$

where $l \in \mathbb{R}$ denotes the air gap between the movable plate and the top electrode, and l_0 the gap when both input voltages V_f and V_b are zero. The corresponding electrostatic forces acting on the movable plate due to the input voltages V_f and V_b are

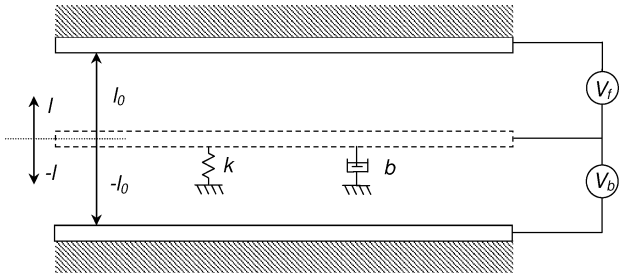

Fig. 1. 1DOF electrostatic micro-actuator with bidirectional drive.

$$F_f = -\frac{1}{2}\frac{\partial C_f}{\partial l}V_f^2 = \frac{\epsilon A}{2(l_0 - l)^2}V_f^2$$
$$F_b = -\frac{1}{2}\frac{\partial C_b}{\partial l}V_b^2 = -\frac{\epsilon A}{2(l_0 + l)^2}V_b^2. \tag{2}$$

Thus, the state-space equations governing the dynamics of the electrostatic microactuator are given by

$$m\ddot{l} + b(l)\dot{l} + kl = \frac{\epsilon A}{2}\left(\frac{V_f^2}{(l_0 - l)^2} - \frac{V_b^2}{(l_0 + l)^2}\right) =: \frac{\epsilon A}{2}\nu \tag{3}$$

where m denotes the mass of the movable electrode, ϵ the permittivity of the gap, A the plate area, k the spring constant, and $b(l)$ the nonlinear squeeze film damping. A simplified form for $b(l)$ obtained from linearization of the compressible Reynolds gas-film equation [27] is

$$b(l) = \frac{b_c}{g^3}. \tag{4}$$

This function, exhibiting a cubic dependence on the air gap g in the denominator has been described in several works [28]–[32], but with different values of the coefficient b_c. In this paper, by averaging the effects of the two layers of squeeze films on both sides of the movable electrode, we arrive at the following modified model

$$b(l) = \frac{b_c}{2}\left(\frac{1}{(l_0 - l)^3} + \frac{1}{(l_0 + l)^3}\right). \tag{5}$$

Although nonlinear squeeze film damping model (5) is considered in this paper, the control design methodology is also applicable to linear damping models as a special case, for both full-state and output feedback problems.

The constant parameters m, ϵ, A, b_c, and k may be difficult to identify accurately in practice, and are thus considered to be uncertain. For example, m, k, and A can vary from unit to unit due to limitations in fabrication precision. The permittivity ϵ can change according to the ambient humidity. The coefficient b_c in the damping model is composed of parameters such as fluid viscosity and plate dimensions, and is thus likely to vary according to ambient conditions and fabrication consistency. Nevertheless, it is reasonable to have good indication of the order of magnitudes of these parameters.

The voltages V_f and V_b are independent inputs which collectively provide controllability of the movable plate in both

directions. By lumping the two voltage terms into an aggregate control variable ν in (3), we can design it as an unconstrained input first, and subsequently apportion it to the actual voltage inputs. In practice, the displacement l can be measured by state-of-the-art capacitive sensing methods (see, e.g., [33]). The only difficulty is in the measurement of the velocity $\dot{l}$, thus motivating the importance of output feedback designs.

To prevent shorting of the electrical circuit, an insulating layer is present in each of the driving electrodes. This also helps to prevent control singularity, which is evident from (3) whenever $|l| = l_0$, causing the input ν to be undefined. Hence, the state space of the system is to be constrained in the set $\chi = \{(l, \dot{l}) \in \mathbb{R}^2 | |l| < l_0 - \delta\}$, where $0 < \delta < l_0$.

While bidirectional parallel plate actuators, as shown in Fig. 1, can be used for both out-of-plane and in-plane applications, out-of-plane bidirectional configurations involve complex fabrication processes, such that the derived benefits need to be weighed against the costs. On the other hand, lateral parallel plate microactuators are much more feasible, as they can be easily fabricated and configured for bidirectional actuation, such as that shown in [34] for optical moving-fiber switches, and that in [35] for positioning of disk drive sliders.

To obtain the same order of magnitude of the variables and thereby avoid numerical problems in simulation, we perform a change of time scale $\tau = \sigma t$ and change of variables $x_1 = l/l_0$, $x_2 = (dl/d\tau)/l_0$, $u = \nu/\beta$, for large constants $\sigma > 0$ and $\beta > 0$, thus yielding the following form of nonlinear dynamics in the strict-feedback form:

$$\begin{aligned} \frac{dx_1}{d\tau} &= x_2(\tau) \\ \frac{dx_2}{d\tau} &= -\frac{b_c}{2m\sigma l_0^3}\bar{b}x_2(\tau) - \frac{k}{m\sigma^2}x_1(\tau) + \frac{\epsilon A\beta}{2m\sigma^2 l_0}u(\tau) \\ y &= x_1(\tau) \end{aligned} \tag{6}$$

where $y \in \mathbb{R}$ is the output and $\bar{b}(x_1)$ is described by

$$\bar{b}(x_1) = \frac{1}{(1-x_1)^3} + \frac{1}{(1+x_1)^3}. \tag{7}$$

For ease of notation, $\dot{x}_1$ and $\dot{x}_2$ are henceforth understood as $dx_1/d\tau$ and $dx_2/d\tau$, respectively, following the change of time scale.

The scaling constants σ and β condition the magnitude of the coefficients. For instance, the large constant σ moderates the value of $k/(m\sigma^2)$, which is otherwise very large and may pose problems in numerical implementation. On the other hand, the coefficient $\epsilon A/(2m\sigma^2 l_0)$ in the second equation of (6) can be very small. By working with the scaled input $u = \nu/\beta$ instead of ν, the large constant β is introduced, which moderates the magnitude of the coefficient for easier simulation. These scalings are introduced for analysis purposes only, and do not change the properties of the original plant (3). The choice of the scaling constants may be motivated by *a priori* knowledge of the order of magnitude of the uncertain parameters.

The control objective is to force the movable electrode to track a reference trajectory $y_d(t)$ within the air gap, i.e., $|y(t) - y_d(t)| \to 0$ as $t \to \infty$, given that $y_d(t)$ satisfies the following assumption.

Assumption 1: The first and second order time-derivatives of the reference trajectory $y_d(t)$ are bounded, i.e., $|\dot{y}_d| < Y_1$, $|\ddot{y}_d| < Y_2$, where Y_1 and Y_2 are constants. In addition, the reference trajectory is bounded by $\underline{y}_d \le y_d(t) \le \overline{y}_d$, where $\underline{y}_d$ and $\overline{y}_d$ are constants that satisfy $\underline{y}_d > -1 + \delta/l_0$ and $\overline{y}_d < 1 - \delta/l_0$.

At the same time, all closed-loop signals are to be kept bounded. To avoid complicated switched systems analysis, we aim to design a control scheme which ensures that the movable plate does not come into contact with the electrodes.

III. Barrier Functions in Lyapunov Synthesis

For clarity of presentation, we outline the method of employing barrier functions [26] in backstepping Lyapunov synthesis to design a control that prevents the system states from violating the constraints. For simplicity, consider the following second-order system:

$$\dot{x}_1 = x_2 \quad \dot{x}_2 = f(x) + u \tag{8}$$

where $x = [x_1, x_2]^T$, and the state x_1 is required to satisfy $|x_1| < k_c$, with k_c being a constant.

Backstepping is a systematic control design procedure for certain classes of nonlinear systems possessing a triangular structure, in particular, parametric strict feedback form [18], for which the plant (6) satisfies. The backstepping procedure employs virtual control laws to stabilize all but the last differential equation and derives the actual control law in the final equation in terms of the virtual controls. In the first step of the procedure, we define the error coordinates $z_1 = x_1 - y_d$ and $z_2 = x_2 - \alpha_1$, where α_1 is a virtual control to be designed. To design a control that does not drive x_1 out of the interval $(-k_c, k_c)$, the following Lyapunov function candidate comprising a barrier function [26] is proposed in the first step of backstepping

$$V_1 = \frac{\kappa_0}{2}\log\frac{k_b}{k_b - z_1^2} \tag{9}$$

where κ_0 is a positive constant, and

$$k_b = \left(k_c - \max\left\{|\overline{y}_d|, |\underline{y}_d|\right\}\right)^2 \tag{10}$$

denotes the constraint on z_1^2, that is, $z_1^2 < k_b$. For clarity of presentation, a schematic illustration of $V_1(z_1)$ is shown in Fig. 2(a).

It can be shown that V_1 is positive definite and continuously differentiable in the open set $|z_1| < \sqrt{k_b}$, and thus a valid Lyapunov function candidate. The derivative of V_1 is given by

$$\dot{V}_1 = \frac{\kappa_0 z_1 \dot{z}_1}{k_b - z_1^2} = \frac{\kappa_0 z_1(z_2 + \alpha_1 - \dot{y}_d)}{k_b - z_1^2}$$

for which the design of virtual control

$$\alpha_1 = -\left(k_b - z_1^2\right)\kappa_1 z_1 + \dot{y}_d$$

where $\kappa_1 > 0$ is a constant, yields

$$\dot{V}_1 = -\kappa_0\kappa_1 z_1^2 + \frac{\kappa_0 z_1 z_2}{k_b - z_1^2}.$$

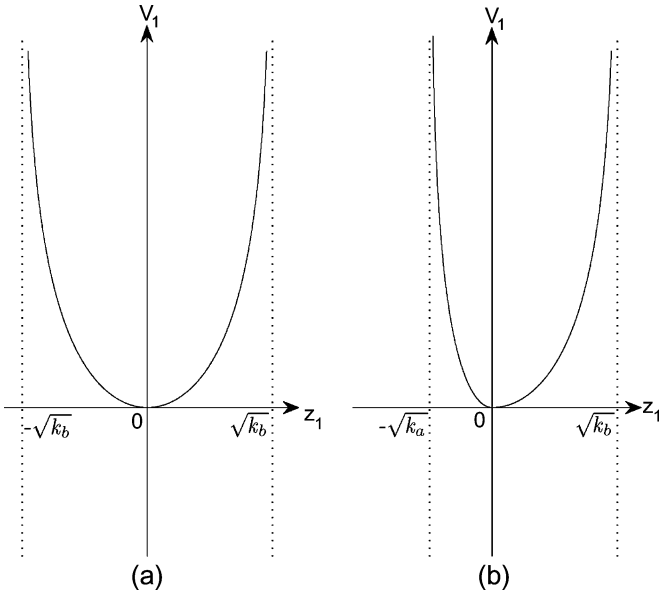

Fig. 2. (a) Schematic illustration of symmetric and (b) asymmetric barrier functions.

In the second step, choose Lyapunov function candidate as follows:

$$V_2 = V_1 + \frac{1}{2}z_2^2 \tag{11}$$

which yields the derivative

$$\dot{V}_2 = -\kappa_0\kappa_1 z_1^2 + \frac{\kappa_0 z_1 z_2}{k_b - z_1^2} + z_2\left(f(x) + u - \dot{\alpha}_1\right)$$

where $\dot{\alpha}_1$ is given by

$$\dot{\alpha}_1 = \kappa_1\left(3z_1^2 - k_b\right)\left[z_2 - \left(k_b - z_1^2\right)\kappa_1 z_1\right] + \ddot{y}_d.$$

By designing the control as

$$u = -\kappa_2 z_2 - f(x) + \dot{\alpha}_1 - \frac{\kappa_0 z_1}{k_b - z_1^2}$$

where $\kappa_2 > 0$ is constant, it can be obtained that

$$\dot{V}_2 = -\kappa_0\kappa_1 z_1^2 - \kappa_2 z_2^2.$$

Since $\dot{V}_2 \leq 0$, it can be shown that $V_2(t)$ is bounded $\forall t > 0$ provided that $V_2(0)$ is bounded and $|z_1(0)| < \sqrt{k_b}$. From (11), it follows that $V_1(t)$ is also bounded. According to (9), we know that for $V_1(t)$ to be bounded, it has to be true that $|z_1(t)| \neq \sqrt{k_b}$. Therefore, the tracking error z_1 remains in the region $|z_1(t)| < \sqrt{k_b}$. Based on Assumption 1, it is clear that the state x_1 remains in the region $|x_1(t)| < k_c$.

Although the example presented previously was for a particular choice of symmetric barrier function $V_1 = (\kappa_0/2)\log(k_b/(k_b - z_1^2))$, we can formalize the result for general forms of barrier functions in Lyapunov synthesis satisfying $V_1(z_1) \to \infty$ as $z_1 \to -\sqrt{k_a}$ or $z_1 \to \sqrt{k_b}$. This is presented in the following lemma, which will be used in the subsequent control design and analysis for the actual system (6).

Lemma 1: For trajectories $z_1(t), z_2(t)$ starting from $z_1(0) \in (-\sqrt{k_a}, \sqrt{k_b})$, $z_2(0) \in \mathbb{R}$, where k_a and k_b are positive constants, if there exists a continuously differentiable and positive definite function

$$V(z_1, z_2) = V_1(z_1) + V_2(z_2) \tag{12}$$

defined on $z_1 \in (-\sqrt{k_a}, \sqrt{k_b})$, $z_2 \in \mathbb{R}$, such that

$$V_1(z_1) \to \infty \text{ as } z_1 \to -\sqrt{k_a} \text{ or } z_1 \to \sqrt{k_b} \tag{13}$$

$$\gamma_1(|z_2|) \leq V_2(z_2) \leq \gamma_2(|z_2|) \tag{14}$$

with γ_1 and γ_2 as class K_∞ functions, and the following inequality holds:

$$\dot{V}(z_1, z_2) \leq 0 \quad \forall\, z_1, z_2 \tag{15}$$

then $z_1(t)$ remains in the open set $z_1 \in (-\sqrt{k_a}, \sqrt{k_b})$ $\forall t > 0$.

Proof: Since $V(z_1, z_2)$ is positive definite and $\dot{V}(z_1, z_2) \leq 0$, it is implied that $V(z_1, z_2)$ is bounded $\forall t > 0$. From $V(z_1, z_2) = V_1(z_1) + V_2(z_2)$ and the fact that $V_1(z_1)$ and $V_2(z_2)$ are positive functions, we can infer that since $V(z_1, z_2)$ is bounded, $V_1(z_1)$ is necessarily bounded as well. Because $V_1(z_1)$ is bounded, we know, from (13), that $z_1 \neq \sqrt{k_b}$ and $z_1 \neq -\sqrt{k_a}$. Given that $-\sqrt{k_a} < z_1(0) < \sqrt{k_b}$, it can be concluded that $z_1(t)$ remains in the open set $-\sqrt{k_a} < z_1 < \sqrt{k_b}$, $\forall t > 0$. ■

IV. Full-State Feedback Adaptive Control Design

Section III outlined a simplified example of how barrier functions are incorporated in Lyapunov synthesis to yield a control which ensures that state constraints are not violated. In this section, we extend the method to investigate full-state feedback adaptive control for uncertain 1DOF electrostatic micro-actuators described by (6).

Step 1: Define error variables $z_1 = x_1 - y_d$ and $z_2 = x_2 - \alpha_1$, where α_1 is the virtual control to be designed. To ensure that the constraint on x_1 is not violated, we consider the following Lyapunov function candidate:

$$V_1 = \frac{\kappa_0}{2}q(z_1)\log\frac{k_b}{k_b - z_1^2} + \frac{\kappa_0}{2}\left(1 - q(z_1)\right)\log\frac{k_a}{k_a - z_1^2} \tag{16}$$

where κ_0 is a positive design constant, the function $q(\cdot) : \mathbb{R} \to \{0, 1\}$ is defined by

$$q(\bullet) = \begin{cases} 1, & \text{if } \bullet > 0 \\ 0, & \text{if } \bullet \leq 0 \end{cases} \tag{17}$$

and

$$k_a = \left(1 - \frac{\delta}{l_0} - |\underline{y}_d|\right)^2 \quad k_b = \left(1 - \frac{\delta}{l_0} - |\overline{y}_d|\right)^2 \tag{18}$$

are positive constants representing the constraints in the z_1 state space, given by $-\sqrt{k_a} < z_1 < \sqrt{k_b}$, induced from the constraints in the x_1 state space, given by $|x_1| < 1 - \delta/l_0$. For clarity of presentation, a schematic illustration of $V_1(z_1)$ is shown in

Fig. 2(b). Throughout this paper, for ease of notation, we abbreviate $q(z_1)$ by q, unless otherwise stated.

Lemma 2: The Lyapunov function candidate $V_1(z_1)$ in (16) is positive definite and continuously differentiable in the open interval $z_1 \in (-\sqrt{k_a}, \sqrt{k_b})$.

Proof: For $0 < z_1 < \sqrt{k_b}$, we have

$$V_1(z_1) = \frac{\kappa_0}{2} \log \frac{k_b}{k_b - z_1^2}$$

and for $-\sqrt{k_a} < z_1 \leq 0$, we have

$$V_1(z_1) = \frac{\kappa_0}{2} \log \frac{k_a}{k_a - z_1^2}.$$

It is easy to see that, for $-\sqrt{k_a} < z_1 < \sqrt{k_b}$, we have that $V_1(z_1) \geq 0$ and that $V_1(z_1) = 0$ if and only if $z_1 = 0$, thus implying that $V_1(z_1)$ is positive definite on the interval.

The function V_1 is piecewise smooth within each of the two intervals $z_1 \in (-\sqrt{k_a}, 0]$ and $z_1 \in (0, \sqrt{k_b})$. Thus, to show that V_1 is a continuously differentiable function, we only need to show that $\lim_{z_1 \to 0} dV_1/dz_1$ is identical from both directions. On the interval $0 < z_1 < \sqrt{k_b}$, we have

$$\lim_{z_1 \to 0^+} \frac{dV_1}{dz_1} = \lim_{z_1 \to 0^+} \frac{\kappa_0 z_1}{k_b - z_1^2} = 0.$$

Similarly, for $-\sqrt{k_a} < z_1 \leq 0$, we obtain that

$$\lim_{z_1 \to 0^-} \frac{dV_1}{dz_1} = \lim_{z_1 \to 0^-} \frac{\kappa_0 z_1}{k_a - z_1^2} = 0.$$

Hence, we conclude that $V_1(z_1)$ is continuously differentiable on the interval $z_1 \in (-\sqrt{k_a}, \sqrt{k_b})$. ■

Remark 1: Note that $V_1(z_1)$ in (16) is designed to handle asymmetrical constraints $-\sqrt{k_a} < z_1 < \sqrt{k_b}$, and is more general than that in (9), which was constructed for symmetrical constraints $|z_1| < \sqrt{k_b}$.

The derivative of V_1 is given by

$$\dot{V}_1 = \left(\frac{q}{k_b - z_1^2} + \frac{1-q}{k_a - z_1^2} \right) \kappa_0 z_1 (z_2 + \alpha_1 - \dot{y}_d)$$

from which we can choose the virtual control as

$$\alpha_1 = -\kappa_1 \left[q\left(k_b - z_1^2\right) + (1-q)\left(k_a - z_1^2\right) \right] z_1^3 + \dot{y}_d \quad (19)$$

with κ_1 being a positive constant, to yield the following:

$$\dot{V}_1 = -\kappa_0 \kappa_1 z_1^4 + \left(\frac{q}{k_b - z_1^2} + \frac{1-q}{k_a - z_1^2} \right) \kappa_0 z_1 z_2$$

where the first term is always non-positive and the second term will be cancelled in the subsequent step.

Lemma 3: The virtual control $\alpha_1(z_1, \dot{y}_d)$ in (19) is continuously differentiable with respect to z_1 on the interval $z_1 \in (-\sqrt{k_a}, \sqrt{k_b})$.

Proof: The virtual control α_1 is piecewise continuously differentiable with respect to z_1 over the two intervals $z_1 \in (-\sqrt{k_a}, 0]$ and $z_1 \in (0, \sqrt{k_b})$. Thus, to show that α_1 is a continuously differentiable function for $-\sqrt{k_a} < z_1 < \sqrt{k_b}$, we need only to show that $\lim_{z_1 \to 0} \partial \alpha_1 / \partial z_1$ is identical from both directions. For $0 < z_1 < \sqrt{k_b}$, we have

$$\lim_{z_1 \to 0^+} \frac{\partial \alpha_1}{\partial z_1} = \lim_{z_1 \to 0^+} \kappa_1 \left(-3k_b + 5z_1^2 \right) z_1^2 = 0.$$

Similarly, for $-\sqrt{k_a} < z_1 \leq 0$, we obtain that

$$\lim_{z_1 \to 0^-} \frac{\partial \alpha_1}{\partial z_1} = \lim_{z_1 \to 0^-} \kappa_1 \left(-3k_a + 5z_1^2 \right) z_1^2 = 0.$$

Hence, $\lim_{z_1 \to 0^+} \partial \alpha_1 / \partial z_1 = \lim_{z_1 \to 0^-} \partial \alpha_1 / \partial z_1$, and we conclude that $\alpha_1(z_1, \dot{y}_d)$ is continuously differentiable with respect to z_1 on the interval $z_1 \in (-\sqrt{k_a}, \sqrt{k_b})$. ■

Remark 2: The virtual control α_1 in (19) is designed to contain the third power of z_1 so as to ensure that its partial derivative $\partial \alpha_1 / \partial z_1$, which will be used in the design of the control law in the subsequent step, is continuous, as shown in Lemma 3. However, if we design the virtual control as

$$\alpha_1 = -\kappa_1 \left[q\left(k_b - z_1^2\right) + (1-q)\left(k_a - z_1^2\right) \right] z_1 + \dot{y}_d$$

then it can be checked that $\lim_{z_1 \to 0^+} \partial \alpha_1 / \partial z_1 \neq \lim_{z_1 \to 0^-} \partial \alpha_1 / \partial z_1$, where it is clear that $\partial \alpha_1 / \partial z_1$ is discontinuous and ill-defined at $z_1 = 0$.

Step 2: This is the step in which the actual control input will be designed. Consider the following Lyapunov function candidate:

$$V_2^* = V_1 + \frac{m\sigma^2 l_0}{\epsilon A \beta} z_2^2 \quad (20)$$

with the following derivative:

$$\dot{V}_2^* = -\kappa_0 \kappa_1 z_1^4 + \left(\frac{q}{k_b - z_1^2} + \frac{1-q}{k_a - z_1^2} \right) \kappa_0 z_1 z_2 + \frac{2m\sigma^2 l_0}{\epsilon A \beta} z_2 \times \left[-\frac{b_c}{2m\sigma l_0^3} \bar{b}(x_1) x_2 - \frac{k}{m\sigma^2} x_1 + \frac{\epsilon A \beta}{2m\sigma^2 l_0} u - \dot{\alpha}_1 \right].$$

From (19), the derivative of α_1 is given by

$$\dot{\alpha}_1 = \kappa_1 \left[-3\left(qk_b + (1-q)k_a\right) + 5z_1^2 \right] z_1^2 (x_2 - \dot{y}_d) + \ddot{y}_d.$$

Ideally, we can design the control input as

$$u = u^* = -\kappa_2 z_2 - \left(\frac{q}{k_b - z_1^2} + \frac{1-q}{k_a - z_1^2} \right) \kappa_0 z_1 + \theta^T \psi \quad (21)$$

where κ_2 is a positive constant, and

$$\theta = \frac{2m\sigma^2 l_0}{\epsilon A \beta} \left[\frac{k}{m\sigma^2},\ \frac{b_c}{2m\sigma l_0^3},\ 1 \right]^T$$
$$\psi = \left[x_1,\ \bar{b}(x_1) x_2,\ \dot{\alpha}_1 \right]^T$$

which leads to the following equation:

$$\dot{V}_2^* = -\kappa_0 \kappa_1 z_1^4 - \kappa_2 z_2^2.$$

Based on this, the asymptotic convergence of the error signals z_1 and z_2 to zero can be shown after some analysis.

However, the ideal control law (21) is not viable due to the fact that the parameters m, ϵ, A, b, and k in θ are not available. To deal with the parametric uncertainty, we employ the certainty-equivalent control law

$$u = -\kappa_2 z_2 - \left(\frac{q}{k_b - z_1^2} + \frac{1-q}{k_a - z_1^2}\right)\kappa_0 z_1 + \hat{\theta}^T \psi \qquad (22)$$

where $\hat{\theta} \in \mathbb{R}^3$ is the estimate of θ. Since u is an aggregate control variable defined for ease of analysis, we still need to compute the actual voltage controls V_f and V_b. Motivated by [24], the control allocation is performed with the following algorithm:

$$V_f = \sqrt{\beta l_0^2 q(u)(1-x_1)^2 u}$$
$$V_b = \sqrt{-\beta l_0^2 (1-q(u))(1+x_1)^2 u} \qquad (23)$$

where the function $q(\cdot)$ is defined in (17). It can be checked that $\beta l_0^2 q(u)(1-x_1)^2 u$ and $-\beta l_0^2(1-q(u))(1+x_1)^2 u$, i.e., the terms within the square root operators, are always non-negative.

For stability analysis and design of the adaptation law, we augment the Lyapunov function candidate with a quadratic term of parametric estimation error as follows:

$$V_2 = V_1 + \frac{m\sigma^2 l_0}{\epsilon A \beta} z_2^2 + \frac{1}{2}\tilde{\theta}^T \Gamma^{-1} \tilde{\theta} \qquad (24)$$

where $\tilde{\theta} = \hat{\theta} - \theta$, and $\Gamma = \Gamma^T > 0$ is a constant matrix. The derivative of V_2 is given by

$$\dot{V}_2 = -\kappa_0 \kappa_1 z_1^4 + \left(\frac{q}{k_b - z_1^2} + \frac{1-q}{k_a - z_1^2}\right)\kappa_0 z_1 z_2 + z_2(-\theta^T \psi + u) + \tilde{\theta}^T \Gamma^{-1} \dot{\hat{\theta}}.$$

Substituting control law (22) into the previous equation, we obtain that

$$\dot{V}_2 = -\kappa_0 \kappa_1 z_1^4 - \kappa_2 z_2^2 + \tilde{\theta}^T \psi z_2 + \tilde{\theta}^T \Gamma^{-1} \dot{\hat{\theta}}.$$

By designing the adaptation law as

$$\dot{\hat{\theta}} = -\Gamma \psi z_2 \qquad (25)$$

it can be shown that the following equation holds:

$$\dot{V}_2 = -\kappa_0 \kappa_1 z_1^4 - \kappa_2 z_2^2. \qquad (26)$$

With the previous equation, we are ready to present our main results in the following theorem.

Theorem 1: Consider the uncertain 1DOF electrostatic micro-actuator system (6) under Assumption 1, full-state feedback control law (22), and adaptation law (25). Starting from initial conditions $(x_1(0), x_2(0)) \in \bar{\Omega} := \{(x_1, x_2) \in \mathbb{R}^2 | y_d(0) - \sqrt{k_a} < x_1 < y_d(0) + \sqrt{k_b}\}$, the output tracking error with respect to any reference trajectory within the air gap, i.e., $y_d \in (-l_0 + \delta, l_0 - \delta)$, is asymptotically stabilized, i.e., $y(t) \to y_d(t)$ as $t \to \infty$, while keeping all closed-loop signals bounded. Furthermore, the output $y(t)$ remains in the set $\Omega_y := \{y \in \mathbb{R} : |y| < 1 - \delta/l_0\}\ \forall t > 0$, i.e., output constraint is never violated.

Proof: First, we show that all closed-loop signals are bounded. From (26), we know that $\dot{V}_2(t) \le 0\ \forall t > 0$, and thus, the error signals $z_1(t)$, $z_2(t)$, and $\tilde{\theta}(t)$ are bounded. Since $\tilde{\theta} = \hat{\theta} - \theta$, and θ is constant, we have that $\hat{\theta}$ is bounded. The boundedness of $z_1(t)$ and the reference trajectory $y_d(t)$ imply that the state $x_1(t)$ is bounded. Given that $\dot{y}_d(t)$ is bounded, the virtual control $\alpha_1(t)$ is also bounded from (19). This leads to the boundedness of state $x_2(t) = z_2(t) + \alpha_1(t)$. According to Lemma 1, we have that $-\sqrt{k_a} < z_1 < \sqrt{k_b}$, which, together with the fact that $\ddot{y}_d(t)$ is bounded, and that $|x_1| < 1 - \delta/l_0$, imply that the control $u(t)$ from (22) is bounded. Therefore, all closed-loop signals are bounded.

Next, we show that $y(t) \to y_d(t)$ as $t \to \infty$. First, we compute $\ddot{V}_2$ as follows:

$$\ddot{V}_2 = -4\kappa_0 \kappa_1 z_1^3 (x_2 - \dot{y}_d) - \frac{\epsilon A \beta}{m\sigma^2 l_0} \kappa_2 z_2 (-\kappa_2 z_2 + \tilde{\theta}^T \psi).$$

From the boundedness of the closed loop signals, it can be shown that $\ddot{V}_2(t)$ is bounded, thus implying that $\dot{V}_2(t)$ is uniformly continuous. Then, by Barbalat's Lemma [13], we obtain that $z_1(t), z_2(t) \to 0$ as $t \to \infty$. Since $z_1(t) = x_1(t) - y_d(t)$, it is clear that $y(t) \to y_d(t)$ as $t \to \infty$.

Last, to show that $y(t) \in \Omega_y\ \forall t > 0$, we employ similar argument as Lemma 1. Note that $\dot{V}_2(t) \le 0\ \forall t > 0$, which implies that for any bounded $V_2(0)$, we have that $V_2(t)$ remains bounded $\forall t > 0$. From (24), it follows that $V_1(t)$ is bounded $\forall t > 0$ and thus $-\sqrt{k_a} < z_1(t) < \sqrt{k_b}$. From (18) and $z_1 = y - y_d$, it can be shown that

$$-1 + \frac{\delta}{l_0} + y_d(t) + |\underline{y}_d| < y(t) < 1 - \frac{\delta}{l_0} + y_d(t) - |\overline{y}_d|.$$

From Assumption 1, we know that $\underline{y}_d \le y_d \le \overline{y}_d$, which yields the fact that $y_d + |\underline{y}_d| \ge 0$ and $y_d - |\overline{y}_d| \le 0$, leading to the following inequality:

$$-1 + \frac{\delta}{l_0} < y < 1 - \frac{\delta}{l_0}.$$

Hence, we can conclude that $y(t) \in \Omega_y\ \forall t > 0$. ■

V. Output Feedback Adaptive Control Design

Full-state feedback control, as presented in Section IV, requires measurements of displacement l and velocity $\dot{l}$. While the displacement l can be measured by state-of-the-art sensors in practice, it is generally difficult to measure the velocity $\dot{l}$ for feedback control. Thus, the state x_1 is available but not x_2. In this section, we present output feedback control design based on adaptive observer backstepping [18].

A. State Transformation and Filter Design

To facilitate the design of the adaptive observer backstepping control, we first perform a change of coordinates

$$\eta_1 = x_1 \qquad (27)$$
$$\eta_2 = x_2 + \frac{b_c}{m\sigma l_0^3} \bar{\phi}(x_1) \qquad (28)$$

where $\bar{\phi}(x_1)$ is defined by

$$\bar{\phi}(x_1) = \frac{1}{2}\left(\frac{1}{(1-x_1)^2} - \frac{1}{(1+x_1)^2}\right). \tag{29}$$

It can be shown that the derivative of $\bar{\phi}$ is given by

$$\begin{aligned}\dot{\bar{\phi}} &= \frac{\partial \bar{\phi}(x_1)}{\partial x_1}\dot{x}_1 = \left(\frac{1}{(1-x_1)^3} + \frac{1}{(1+x_1)^3}\right)x_2 \\ &=: \bar{b}(x_1)x_2. \end{aligned} \tag{30}$$

Substituting (27)–(30) into (6), we can rewrite the system dynamics into the parametric output feedback form

$$\begin{aligned}\dot{\eta}_1 &= \eta_2 - \theta_1\bar{\phi}(\eta_1) \\ \dot{\eta}_2 &= -\theta_2\eta_1 + \vartheta u \\ y &= \eta_1\end{aligned}$$

where $\theta_1 = b_c/(m\sigma l_0^3)$, $\theta_2 = k/(m\sigma^2)$, $\vartheta = \epsilon A\beta/(2m\sigma^2 l_0)$. This can be represented by the simplified form

$$\dot{\eta} = A\eta + \sum_{i=1}^{2}\theta_i\phi_i(y) + \vartheta e_2 u \quad y = \eta_1$$

where $e_2 := [0,1]^T$, $\eta = [\eta_1, \eta_2]^T$, $A = \begin{bmatrix}0 & 1\\ 0 & 0\end{bmatrix}$, $\phi_1(y) = [-\bar{\phi}(y), 0]^T$, $\phi_2(y) = [0, -y]^T$.

Design the following filters:

$$\dot{\xi}_0 = A_0\xi_0 + cy \tag{31}$$

$$\dot{\xi}_i = A_0\xi_i + \phi_i(y), \quad i = 1,2 \tag{32}$$

$$\dot{v} = A_0 v + e_2 u + \varphi \tag{33}$$

where $\xi_i = [\xi_{i1}, \xi_{i2}]^T \in \mathbb{R}^2$ (i = 0,1,2) and $v = [v_1, v_2]^T \in \mathbb{R}^2$ are filter states, $\varphi(\cdot) = [\varphi_1, \varphi_2]^T \in \mathbb{R}^2$ is a correction function to be designed, and $c = [c_1, c_2]^T$ with positive constants c_1 and c_2 chosen such that the matrix

$$A_0 = \begin{bmatrix}-c_1 & 1\\ -c_2 & 0\end{bmatrix}$$

satisfies

$$A_0^T P + PA_0 = -R \tag{34}$$

for some $P = P^T > 0$ and $R = R^T > 0$.

Remark 3: It is necessary to implement the filters (31)–(33) due to the problems associated with reconstructing the states using certainty equivalence methods, namely that the observation error dynamics will be corrupted by parameter estimation errors. As will be shown subsequently, the use of these filters renders the observation error dynamics almost autonomous, if not for the correction term $\varphi(\cdot)$, which will be systematically designed to guarantee closed-loop stability.

By constructing the state estimate as follows:

$$\hat{\eta}(t) = \xi_0(t) + \sum_{i=1}^{2}\theta_i\xi_i(t) + \vartheta v(t)$$

it is easy to see that the dynamics of the observation error, $\tilde{\eta} = \hat{\eta} - \eta$, are given by

$$\dot{\tilde{\eta}} = A_0\tilde{\eta} + \vartheta\varphi$$

which is almost autonomous observation error dynamics, except for the correction term $\varphi(\cdot)$, which will be designed later. The constructive procedure for adaptive observer backstepping design will be presented next.

B. Adaptive Observer Backstepping

The method presented in this section is similar to the backstepping procedure in Section IV, but the filter signal v_2 of (33) is used as the virtual control, instead of the state x_2, which is unavailable.

Step 1: Define $z_1 = y - y_d$, whose derivative is given by

$$\dot{z}_1 = \xi_{02} + \sum_{i=1}^{2}\theta_i\xi_{i2} + \vartheta v_2 - \tilde{\eta}_2 - \theta_1\bar{\phi}(y) - \dot{y}_d \tag{35}$$

where ξ_{ij} and v_j denote the jth elements of ξ_i and v, respectively. Denote $z_2 = v_2 - \alpha_1$, where α_1 is a virtual control to be designed, and consider the Lyapunov function candidate

$$\begin{aligned}V_1 = &\frac{\kappa_0}{2}q(z_1)\log\frac{k_b}{k_b - z_1^2} + \frac{\kappa_0}{2}(1 - q(z_1))\log\frac{k_a}{k_a - z_1^2} \\ &+ \frac{1}{2}\tilde{\Theta}_1^T\Gamma_1^{-1}\tilde{\Theta}_1 + \frac{\vartheta}{2\gamma_\varrho}\tilde{\varrho}^2\end{aligned} \tag{36}$$

where $\Theta_1 = [\theta_1, \theta_2]^T$, and $\tilde{\Theta}_1 = \hat{\Theta}_1 - \Theta_1$ is the estimation error. The derivative of V_1 is given by

$$\begin{aligned}\dot{V}_1 = &\left(\frac{q}{k_b - z_1^2} + \frac{1-q}{k_a - z_1^2}\right)\kappa_0 z_1\left[\xi_{02} + \Theta_1^T\Psi_1\right. \\ &\left.+\vartheta(z_2 + \alpha_1) - \tilde{\eta}_2 - \dot{y}_d\right] + \tilde{\Theta}_1^T\Gamma_1^{-1}\dot{\hat{\Theta}}_1 + \frac{\vartheta}{\gamma_\varrho}\tilde{\varrho}\dot{\hat{\varrho}}\end{aligned}$$

where $\Psi_1 = [\xi_{12} - \bar{\phi}(y), \xi_{22}]^T$. Denote $\hat{\varrho}$ as the estimate of $\varrho = 1/\vartheta$, with $\tilde{\varrho} = \hat{\varrho} - \varrho$ as the estimation error, and let the virtual control $\alpha_1 = \hat{\varrho}\bar{\alpha}_1$, where $\bar{\alpha}_1$ is to be defined shortly. Hence, the previous equation can be rewritten as

$$\begin{aligned}\dot{V}_1 = &\left(\frac{q}{k_b - z_1^2} + \frac{1-q}{k_a - z_1^2}\right) \\ &\times \kappa_0 z_1\left(\xi_{02} + \bar{\alpha}_1 + \Theta_1^T\Psi_1 + \hat{\vartheta}z_2 - \dot{y}_d\right) + \tilde{\Theta}_1^T\Gamma_1^{-1}\dot{\hat{\Theta}}_1 \\ &+ \left(\frac{q}{k_b - z_1^2} + \frac{1-q}{k_a - z_1^2}\right)\kappa_0(-z_1\tilde{\eta}_2 - \tilde{\vartheta}z_1 z_2) \\ &+ \vartheta\tilde{\varrho}\left[\left(\frac{q}{k_b - z_1^2} + \frac{1-q}{k_a - z_1^2}\right)\kappa_0\bar{\alpha}_1 z_1 + \frac{1}{\gamma_\varrho}\dot{\hat{\varrho}}\right].\end{aligned} \tag{37}$$

The virtual control is designed as

$$\alpha_1 = \hat{\varrho}\bar{\alpha}_1 \tag{38}$$

where

$$\begin{aligned}\bar{\alpha}_1 := &-\left[q\left(k_b - z_1^2\right) + (1-q)\left(k_a - z_1^2\right)\right]\kappa_1 z_1^3 \\ &- \xi_{02} - \hat{\Theta}_1^T\Psi_1 + \dot{y}_d\end{aligned} \tag{39}$$

while the adaptation laws are given by

$$\dot{\hat{\Theta}}_1 = \Gamma_1 \Psi_1 \left(\frac{q}{k_b - z_1^2} + \frac{1-q}{k_a - z_1^2} \right) \kappa_0 z_1 \tag{40}$$

$$\dot{\hat{\varrho}} = -\gamma_\varrho \left(\frac{q}{k_b - z_1^2} + \frac{1-q}{k_a - z_1^2} \right) \kappa_0 \bar{\alpha}_1 z_1. \tag{41}$$

Substituting the virtual control and adaptation laws (38)–(41) into (37) yields the following:

$$\dot{V}_1 = -\kappa_0 \kappa_1 z_1^4 + \left(\frac{q}{k_b - z_1^2} + \frac{1-q}{k_a - z_1^2} \right) \times \kappa_0 (\hat{\vartheta} z_1 z_2 - z_1 \tilde{\eta}_2 - \tilde{\vartheta} z_1 z_2). \tag{42}$$

From (42), it can be seen that the first term is stabilizing, while the second term consisting of state and parameter estimation errors will be brought forward into the subsequent step to be handled by the actual control. Similar to Lemma 3, we assert that $\partial \alpha_1 / \partial z_1$ is a continuous function in the following lemma.

Lemma 4: The virtual control α_1, defined in (38), is continuously differentiable with respect to z_1 on the interval $z_1 \in (-\sqrt{k_a}, \sqrt{k_b})$.

Proof: Since α_1 is piecewise continuously differentiable with respect to z_1 over the two intervals $z_1 \in (-\sqrt{k_a}, 0]$ and $z_1 \in (0, \sqrt{k_b})$, and $\lim_{z_1 \to 0^+} \partial \alpha_1 / \partial z_1 = \lim_{z_1 \to 0^-} \partial \alpha_1 / \partial z_1$, we conclude that α_1 is continuously differentiable with respect to z_1 on the interval $z_1 \in (-\sqrt{k_a}, \sqrt{k_b})$. ∎

Step 2: This is the second and final step of the backstepping procedure, in which the control input u appears. According to Lemma 4, the derivative of the virtual control $\alpha_1(\xi_0, \xi_1, \xi_2, z_1, \hat{\Theta}_1, \hat{\varrho}, y_d, \dot{y}_d)$ is well-defined, and can be computed as the sum of the following two parts:

$$\dot{\alpha}_1 = F(\xi_0, \xi_1, \xi_2, z_1, \hat{\Theta}_1, \hat{\varrho}, y_d, \dot{y}_d) + G(\theta_1, \theta_2, \vartheta, \tilde{\eta})$$

in which $F(\cdot)$ is known and can be directly cancelled by the control u, while $G(\cdot)$ contains unknown elements. The functions $F(\cdot)$ and $G(\cdot)$ are defined as follows:

$$\begin{aligned} F =& \frac{\partial \alpha_1}{\partial \xi_0}(A_0 \xi_0 + cy) + \sum_{i=1}^{2} \frac{\partial \alpha_1}{\partial \xi_i}(A_0 \xi_i + \phi_i) \\ &+ \frac{\partial \alpha_1}{\partial \hat{\Theta}_1} \Gamma_1 \Psi_1 \left(\frac{q}{k_b - z_1^2} + \frac{1-q}{k_a - z_1^2} \right) \kappa_0 z_1 \\ &- \frac{\partial \alpha_1}{\partial \hat{\varrho}} \gamma_\varrho \left(\frac{q}{k_b - z_1^2} + \frac{1-q}{k_a - z_1^2} \right) \kappa_0 \bar{\alpha}_1 z_1 \\ &+ \frac{\partial \alpha_1}{\partial z_1}(\xi_{02} - \dot{y}_d) + \sum_{i=0}^{1} \frac{\partial \alpha_1}{\partial y_d^{(i)}} y_d^{(i+1)} \\ =& \hat{\varrho} \omega - \gamma_\varrho \left(\frac{q}{k_b - z_1^2} + \frac{1-q}{k_a - z_1^2} \right) \kappa_0 \bar{\alpha}_1^2 z_1 \end{aligned} \tag{43}$$

$$\begin{aligned} G =& \frac{\partial \alpha_1}{\partial z_1} \left(\sum_{i=1}^{2} \theta_i \xi_{i2} + \vartheta v_2 - \tilde{\eta}_2 - \theta_1 \bar{\phi}(y) \right) \\ =& \frac{\partial \alpha_1}{\partial z_1} \left(\Theta_2^T \Psi_2 - \tilde{\eta}_2 \right) \end{aligned} \tag{44}$$

where $\Theta_2 = [\theta_1, \theta_2, \vartheta]^T$, $\Psi_2 = [\xi_{12} - \bar{\phi}(y), \xi_{22}, v_2]^T$, $\Psi_{1,a} = [c_2 \xi_{11} + \xi_{02} \bar{b}(y), c_2 \xi_{21} + y]^T$, and

$$\begin{aligned} \omega =& c_2(\xi_{01} - y) + \ddot{y}_d + \hat{\Theta}_1^T \Psi_{1,a} \\ &+ \left[-3(qk_b + (1-q)k_a) \kappa_1 z_1^2 + 5\kappa_1 z_1^4 \right] (\xi_{02} - \dot{y}_d) \\ &- \Psi_1^T \Gamma_1 \Psi_1 \left(\frac{q}{k_b - z_1^2} + \frac{1-q}{k_a - z_1^2} \right) \kappa_0 z_1. \end{aligned} \tag{45}$$

This yields the derivative of z_2 as

$$\dot{z}_2 = -c_2 v_1 + u + \varphi_2 - F(\cdot) + \frac{\partial \alpha_1}{\partial z_1} \left(\Theta_2^T \Psi_2 + \tilde{\eta}_2 \right). \tag{46}$$

Consider the Lyapunov function candidate

$$V_2 = V_1 + \frac{1}{2} z_2^2 + \frac{1}{2\vartheta} \tilde{\eta}^T P \tilde{\eta} + \frac{1}{2\gamma_\vartheta} \tilde{\vartheta}^2 + \frac{1}{2} \tilde{\Theta}_2^T \Gamma_2^{-1} \tilde{\Theta}_2 \tag{47}$$

where $\tilde{\Theta}_2 = \hat{\Theta}_2 - \Theta_2$ is the estimation error for the unknown parameter vector Θ_2. Noting (46) and (34), the derivative of V_2 is given by

$$\begin{aligned} \dot{V}_2 =& -\kappa_0 \kappa_1 z_1^4 - \frac{1}{2\vartheta} \tilde{\eta}^T R \tilde{\eta} + \tilde{\Theta}_2^T \left(\Gamma_2^{-1} \dot{\hat{\Theta}}_2 + \frac{\partial \alpha_1}{\partial z_1} \Psi_2 z_2 \right) \\ &+ \tilde{\vartheta} \left[-\left(\frac{q}{k_b - z_1^2} + \frac{1-q}{k_a - z_1^2} \right) \kappa_0 z_1 z_2 + \frac{1}{\gamma_\vartheta} \dot{\hat{\vartheta}} \right] \\ &+ z_2 \left[u + \hat{\vartheta} \left(\frac{q}{k_b - z_1^2} + \frac{1-q}{k_a - z_1^2} \right) \kappa_0 z_1 - c_2 v_1 \right. \\ &\left. + \varphi_2 - F(\cdot) - \frac{\partial \alpha_1}{\partial z_1} \hat{\Theta}_2^T \Psi_2 \right] \\ &+ \tilde{\eta}^T \left[P\varphi + e_2 \left(\frac{\partial \alpha_1}{\partial z_1} z_2 - \left(\frac{q}{k_b - z_1^2} + \frac{1-q}{k_a - z_1^2} \right) \kappa_0 z_1 \right) \right]. \end{aligned} \tag{48}$$

From (48), it can be seen that the last term containing the observation error $\tilde{\eta}$ may be eliminated by choosing the correction term φ as

$$\varphi = -P^{-1} e_2 \left[\frac{\partial \alpha_1}{\partial z_1} z_2 - \left(\frac{q}{k_b - z_1^2} + \frac{1-q}{k_a - z_1^2} \right) \kappa_0 z_1 \right]. \tag{49}$$

By designing the control and adaptation laws as follows:

$$\begin{aligned} u =& -\kappa_2 z_2 + c_2 v_1 - \hat{\vartheta} \left(\frac{q}{k_b - z_1^2} + \frac{1-q}{k_a - z_1^2} \right) \kappa_0 z_1 \\ &+ F(\cdot) - \varphi_2 + \frac{\partial \alpha_1}{\partial z_1} \hat{\Theta}_2^T \Psi_2 \end{aligned} \tag{50}$$

$$\dot{\hat{\Theta}}_2 = -\Gamma_2 \Psi_2 \frac{\partial \alpha_1}{\partial z_1} z_2 \tag{51}$$

$$\dot{\hat{\vartheta}} = \gamma_\vartheta \left(\frac{q}{k_b - z_1^2} + \frac{1-q}{k_a - z_1^2} \right) \kappa_0 z_1 z_2 \tag{52}$$

and substituting (50)–(52) into (48), it can be shown that

$$\dot{V}_2 = -\kappa_0 \kappa_1 z_1^4 - \kappa_2 z_2^2 - \frac{1}{2\vartheta} \tilde{\eta}^T R \tilde{\eta} \tag{53}$$

in which all three terms on the right-hand side are always nonpositive.

Since u is an aggregate control variable defined for ease of analysis, we compute the actual voltage controls V_f and V_b by using the algorithm in (23).

Remark 4: It can be checked that the control $u = u(y, v, \xi_0, \xi_1, \xi_2, \hat{\Theta}_1, \hat{\Theta}_2, \hat{\varrho}, \hat{\vartheta}, y_d, \dot{y}_d, \ddot{y}_d)$, where the filter signals $\xi_0(t)$, $\xi_1(t)$, $\xi_2(t)$ are generated from $y(t)$, the signal $v(t)$ from $u(t)$, the parameter estimates $\hat{\Theta}_1$, $\hat{\Theta}_2$, $\hat{\varrho}$, $\hat{\vartheta}$ from y, y_d, $\dot{y}_d$, ξ_0, ξ_1, ξ_2. Therefore, the control u is feasible based on only output measurement, and does not require the feedback of the state x_2, which is difficult to measure.

Theorem 2: Consider the uncertain 1DOF electrostatic micro-actuator system (6) under Assumption 1, output feedback control law (50), and adaptation laws (40), (41), (51), and (52). Starting from initial conditions $(x_1(0), x_2(0)) \in \bar{\Omega} := \{(x_1, x_2) \in \mathbb{R}^2 | y_d(0) - \sqrt{k_a} < x_1 < y_d(0) + \sqrt{k_b}\}$, the output tracking error with respect to any reference trajectory within the air gap, i.e., $y_d \in (-l_0 + \delta, l_0 - \delta)$, can be asymptotically stabilized, i.e., $y(t) \to y_d(t)$ as $t \to \infty$, while keeping all closed-loop signals bounded. Furthermore, the output $y(t)$ remains in the set $\Omega_y := \{y \in \mathbb{R} : |y| < 1 - \delta/l_0\}\ \forall t > 0$, i.e., output constraint is never violated.

Proof: First, we show that all closed-loop signals are bounded. From (53), we know that $\dot{V}_2(t) \leq 0\, \forall t > 0$, and thus, the error signals $z_1(t)$, $z_2(t)$, $\tilde{\Theta}_1(t)$, $\tilde{\Theta}_2(t)$, $\tilde{\varrho}(t)$, $\tilde{\vartheta}(t)$, and $\tilde{\eta}(t)$ are bounded. Since Θ_1, Θ_2, ϱ, ϑ are constants, we have that $\hat{\Theta}_1(t)$, $\hat{\Theta}_2(t)$, $\hat{\varrho}(t)$, $\hat{\vartheta}(t)$ are bounded. Since $|x_1| < 1 - \delta/l_0$, we know, from the filters (31), (32), that $\xi_i(t)$ $(i = 0, 1, 2)$ are all bounded.

Given that $\dot{y}_d(t)$ is bounded, the virtual control α_1 is also bounded from (38). This leads to the boundedness of $v_2(t) = z_2(t) + \alpha_1(t)$. According to Lemma 1, the tracking error z_1 remains in the set $-\sqrt{k_a} < z_1 < \sqrt{k_b}$. As such, the adaptation rates $\dot{\hat{\Theta}}_1$, $\dot{\hat{\varrho}}$, $\dot{\hat{\Theta}}_2$, $\dot{\hat{\vartheta}}$ in (40), (41), (51), (52), respectively, are all bounded. Furthermore, we can deduce, from (49), that $\varphi(t)$ is bounded. From (33), we have that $\dot{v}_1 = -c_1 v_1 + v_2 + \varphi_1$, which allows us to see that $v_1(t)$ is also bounded. Thus, we can deduce that the control $u(t)$ in (50) is bounded. At the same time, from (35), it follows that $\hat{\eta}(t)$ is bounded, which in turn implies that $\eta_2(t)$, and thus $x_2(t)$, are bounded. Therefore, all closed-loop signals are bounded.

To prove that $y(t) \to y_d$ as $t \to \infty$, we first compute $\ddot{V}_2$ as follows:

$$\ddot{V}_2 = -4\kappa_1 z_1^3 \dot{z}_1 - 2\kappa_2 z_2 \dot{z}_2 - 2\tilde{\eta}^T R \dot{\tilde{\eta}}.$$

Since all closed-loop signals are bounded, it can be shown that $\dot{z}_1$ is bounded from (35), $\dot{z}_2$ is bounded from (46), and $\dot{\tilde{\eta}}$ is bounded from (35). Hence, $\dot{V}_2(t)$ is bounded, implying that $\dot{V}(t)$ is uniformly continuous. According to Barbalat's Lemma [13], $z_1(t), z_2(t) \to 0$ as $t \to \infty$. Since $z_1(t) = x_1(t) - y_d(t)$, it is clear that $y(t) \to y_d(t)$ as $t \to \infty$.

The proof for $y(t) \in \Omega_y$ is similar to that presented in Theorem 1 and is omitted. ∎

Remark 5: The possible rapid change of control voltages near the electrode surfaces can be viewed as a tradeoff from the ability of the controller to prevent electrode contacts in a relatively simple and robust way, particularly in face of model uncertainty and lack of velocity measurements. Since electrical dynamics are much faster than mechanical dynamics even in the micro scale, the plant model considered is still reasonable. If necessary, upper bounds for the rate of change of control voltages can always be computed for given design constants and initial conditions. From these estimates, the design constants and/or initial conditions can be appropriately selected to curb excessive rates.

Remark 6: In practice, measurement noise may cause problems due to the high sensitivity near the barrier. Low pass filter can be employed to attenuate high frequency measurement noise. Furthermore, we propose to modify the barrier limits, k_a and k_b, into the following:

$$k_a' = \left(1 - \frac{\delta}{l_0} - |\underline{y}_d| - \Delta\right)^2 \quad k_b' = \left(1 - \frac{\delta}{l_0} - |\overline{y}_d| - \Delta\right)^2 \tag{54}$$

so as to provide for a safety margin Δ, which accounts for measurement variance induced by noise. For small noise, we can reasonably expect that the filtered tracking error, denoted by z_1' remains in the interval $(-\sqrt{k_a'}, -\sqrt{k_b'})$. Then, for $|z_1'| \leq |z_1| + \Delta$, we expect that z_1 remains in the interval $(-\sqrt{k_a}, \sqrt{k_b})$. In the subsequent section, we present simulation results to show that closed loop performance under these modifications are robust to small magnitude sensor noise.

VI. Simulation Results

To demonstrate the effectiveness of the control design, we perform simulations on plant (6), for both full-state feedback and output feedback cases, under the following choices of plant parameters values: $b_c = 2.659 \times 10^{-21}$ N · m^2 s, $k = 350$ N · m^{-1}, $m = 1.864 \times 10^{-11}$ kg, $\epsilon = 8.859 \times 10^{-12}$ Fm^{-1}, $A = 2 \times 10^{-8}$ m^2, $l_0 = 1 \times 10^{-6}$ m, $\delta = 2 \times 10^{-8}$ m, and the scaling constants are chosen as $\sigma = 1 \times 10^6$ and $\beta = 2 \times 10^{17}$. The initial conditions are $x_1(0) = x_2(0) = \hat{\theta}_1(0) = \hat{\theta}_2(0) = 0$.

The performance of the proposed control is investigated for two types of tasks: set point regulation and trajectory tracking. For each task, the controller is required to ensure that the condition $-\sqrt{k_a} < z_1 < \sqrt{k_b}$ holds, thereby preventing electrode contact, i.e., $|x_1| < 0.98$.

For set point regulation, the movable plate is required to be stabilized at the specified set points y_{si}, $i = 1, 2, 3, 4$. Between the start position and each set point, the plate is to follow a reference trajectory $y_{di}(t)$ defined by

$$y_{di}(t) = \begin{cases} y_0 + (y_{si} - y_0) d(t), & \text{for } t \leq t_{di} \\ y_{si}, & \text{for } t > t_{di} \end{cases} \tag{55}$$

where $d(t) = 6(t/t_{di})^5 - 15(t/t_{di})^4 + 10(t/t_{di})^3$, y_0 is the desired initial position, and t_d is the time to reach y_s, starting from y_0. We simulate stabilization to four set points within the gap, namely $y_{s1} = -0.2$, $y_{s2} = 0.4$, $y_{s3} = -0.6$, and $y_{s4} = 0.8$, with each case starting from $y_0 = 0.0$. The duration is specified as $t_d = 100$ μs. The bounds on z_1 corresponding to the set points can be computed as $\sqrt{k_{a1}} = 0.78$, $\sqrt{k_{b1}} = 0.98$, $\sqrt{k_{a2}} = 0.98$, $\sqrt{k_{b2}} = 0.58$, $\sqrt{k_{a3}} = 0.38$, $\sqrt{k_{b3}} = 0.98$, $\sqrt{k_{a4}} = 0.98$, and $\sqrt{k_{b4}} = 0.18$.

For trajectory tracking, the movable plate is required to follow the sinusoidal reference trajectory

$$y_d(t) = 0.4\,(\sin(0.1t) + \sin(0.2t)) \tag{56}$$

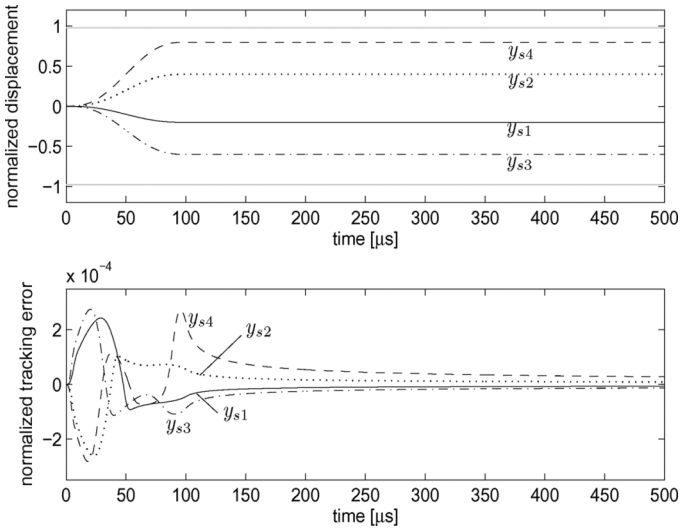

Fig. 3. Full-state feedback tracking performance with respect to different setpoints.

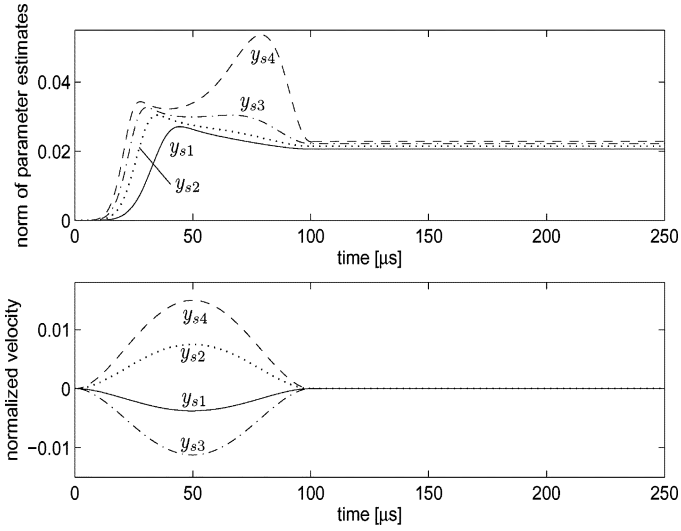

Fig. 5. Norm of parameter estimates and normalized velocity x_2 in full-state feedback setpoint regulation task.

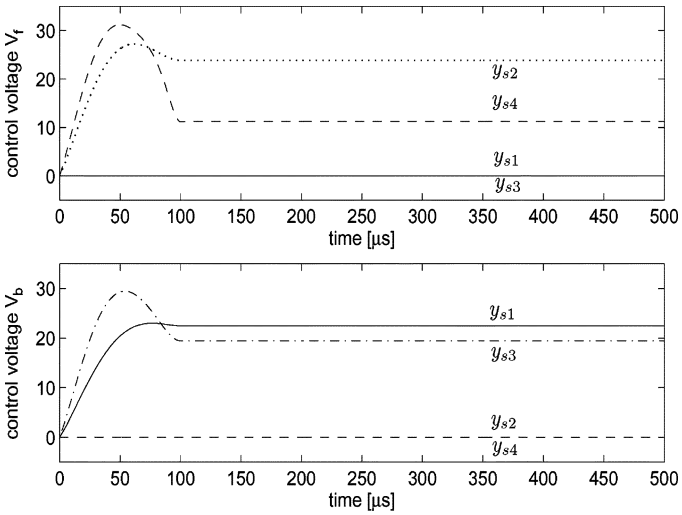

Fig. 4. Control inputs V_f and V_b in full-state feedback setpoint regulation task.

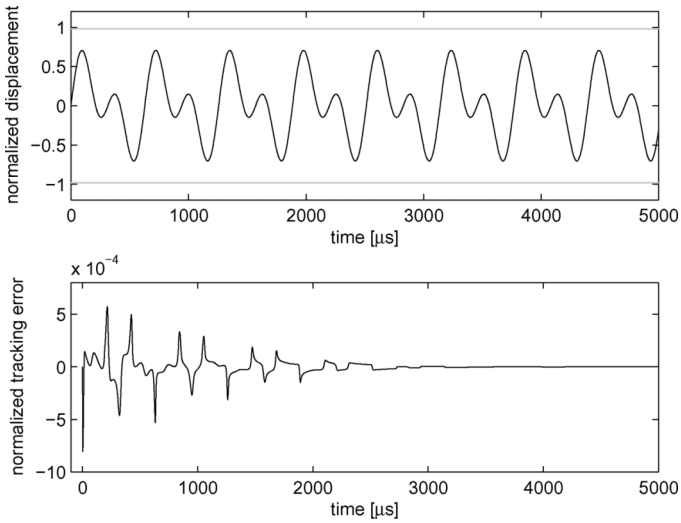

Fig. 6. Full-state feedback tracking performance with respect to sinusoidal reference trajectory.

from which it can be computed that $|\overline{y}_d| = |\underline{y}_d| = 0.705$. Thus, we have $\sqrt{k_a} = \sqrt{k_b} = 1 - 0.02 - 0.705 = 0.275$.

A. Full-State Feedback Control

The full-state feedback control, according to (3), (22), and (23), have design parameters chosen as $\kappa_0 = 1 \times 10^{-3}$, $\kappa_1 = 5 \times 10^7$, $\kappa_2 = 1$, and $\Gamma = \mathrm{diag}\{70, 100, 50\}$.

For set point regulation, the simulation results are shown in Figs. 3–5. From Fig. 3, it can be seen that the movable electrode is successfully stabilized at each of the four set points, and does not come into contact with the fixed electrodes, whose positions are indicated by the grey lines. The tracking error for each case decays to a small value. From Fig. 4, the boundedness and reciprocating action of the two control voltages are shown. Fig. 5 shows that the velocity and parameter estimates are bounded.

Simulation results for the trajectory tracking are detailed in Figs. 6–8. From Fig. 6, it can be seen that the movable plate followed the sinusoidal trajectory closely, and successfully avoided contact with the electrodes. The tracking error $z_1 = x_1 - y_d$ showed a trend of decreasing asymptotically to zero, while not violating the constraint $-0.275 < z_1 < 0.275$ during the transient response. From Fig. 7, the boundedness and reciprocating action of the two control voltages are shown. Fig. 8 shows that the velocity and parameter estimates are bounded.

B. Output Feedback Control

The output feedback control, according to (3), (23), and (50), have design parameters chosen as $\kappa_0 = 1$, $\kappa_1 = \kappa_2 = 2$, $\Gamma_1 = \mathrm{diag}\{60, 10\}$, $\Gamma_2 = 10I$, $\gamma_\varrho = \gamma_\vartheta = 1$, $c_1 = 8$, $c_2 = 15$, and $R = I$.

For the task of set point regulation, it can be seen, from Fig. 9, that the movable electrode is successfully stabilized at each of the four set points without coming into contact with the electrodes. For the task of sinusoidal tracking, the movable plate followed the sinusoidal trajectory closely without contacting the electrodes, as seen in Fig. 10. The tracking error $z_1 = y - y_d$

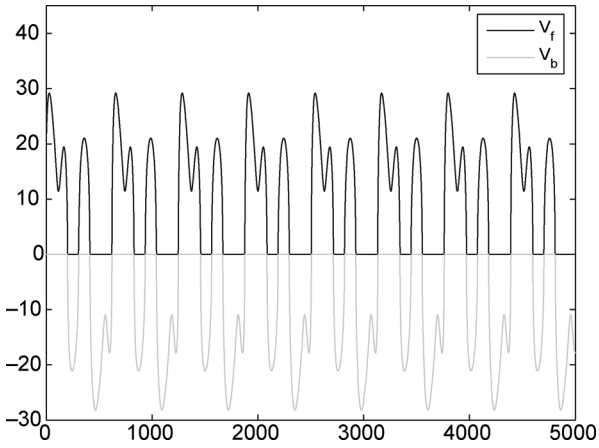

Fig. 7. Control inputs V_f and V_b in full-state feedback trajectory tracking task.

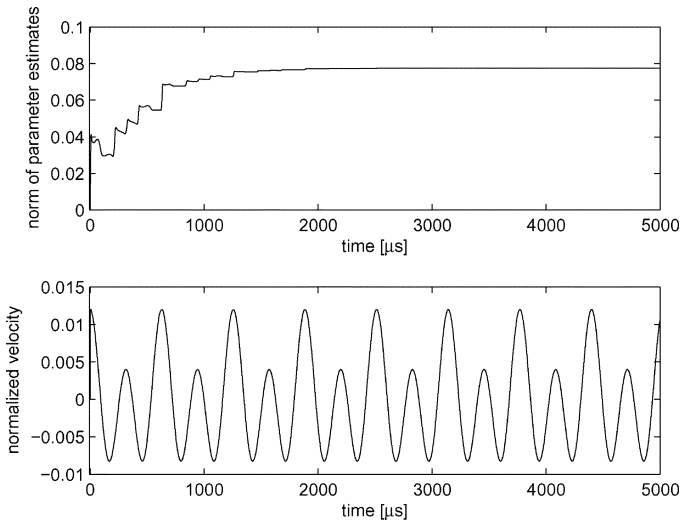

Fig. 8. Norm of parameter estimates and normalized velocity x_2 in full-state feedback trajectory tracking task.

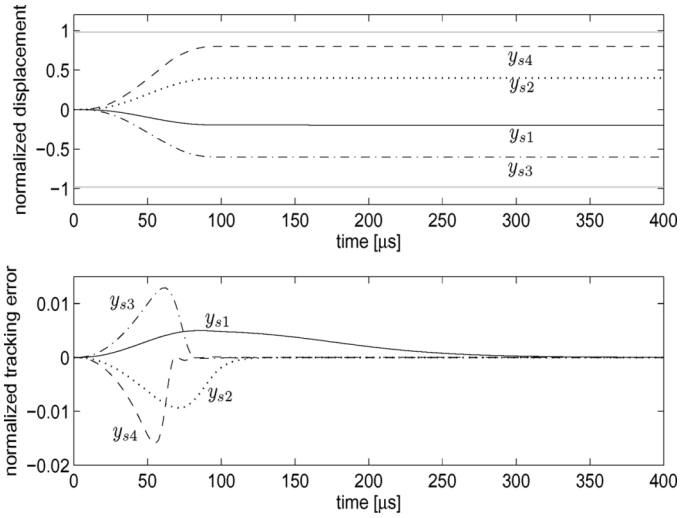

Fig. 9. Output feedback tracking performance with respect to different set-points.

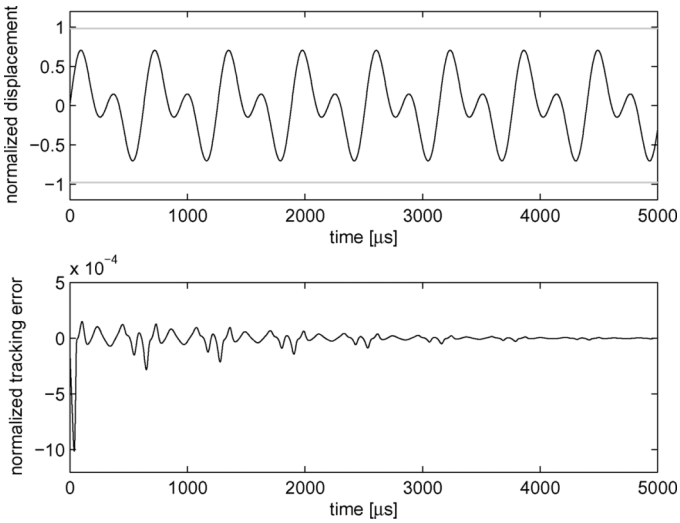

Fig. 10. Output feedback tracking performance with respect to sinusoidal reference trajectory.

decreased rapidly to a small value without violating the constraint $-0.275 < z_1 < 0.275$ during the transient response. Our simulation study also revealed that control voltages, velocity, and parameter estimates are bounded, although these have been omitted in view of space constraints.

C. Measurement Noise

To test the effectiveness of the controller in the presence of sensor noise, we inject noise into the output, such that the measured signal is given by

$$y_m = y + n_a \mu(t)$$

where $\mu \in [-1, 1]$ is a random variable with uniform distribution, and n_a is the noise magnitude. The raw signal y_m is passed through a low pass filter $1/(1+2s)$, where s is the Laplace variable, and the output of the filter, y_f, is then used in the estimation filters, adaptation laws, and control law. The barrier limits are modified according to (54) with $\Delta = 0.05$ so as to provide a safety margin that accounts for measurement variance induced by noise. This yields $\sqrt{k_a'} = \sqrt{k_b'} = 0.27$.

Simulation results for the output feedback tracking control are shown in Figs. 11 and 12 for $n_a = 0.06$ and $n_a = 0.1$, respectively. It can be seen that the effect of the controller is to minimize the filtered tracking error $z_1' = y_f - y_d$ instead of the actual tracking error $z_1 = y_- y_d$. As a result, the actual trajectory y fluctuates about the desired trajectory y_d. As noise magnitude, n_a, increases, the actual tracking error also increases. From the fact that $z_1'(t) \in (-0.27, 0.27)$, it is ensured that $z_1(t) \in (-0.275, 0.275)$, since $|z_1'| \leq |z_1| + 0.05$. This in turn ensures that the true position does not violate constraints, i.e., $|y| < 0.98$.

VII. Conclusion

This paper has presented adaptive control for a class of 1DOF electrostatic micro-actuator systems with bidirectional drive, such that the movable electrode is able to track a reference trajectory within the air gap without knowledge of the plant parameters nor physical contact with any of the fixed electrodes.

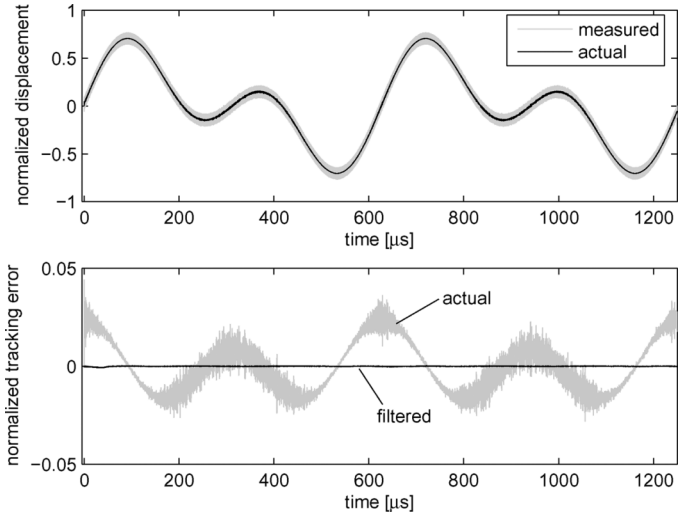

Fig. 11. Tracking performance in presence of measurement noise with $n_a = 0.06$.

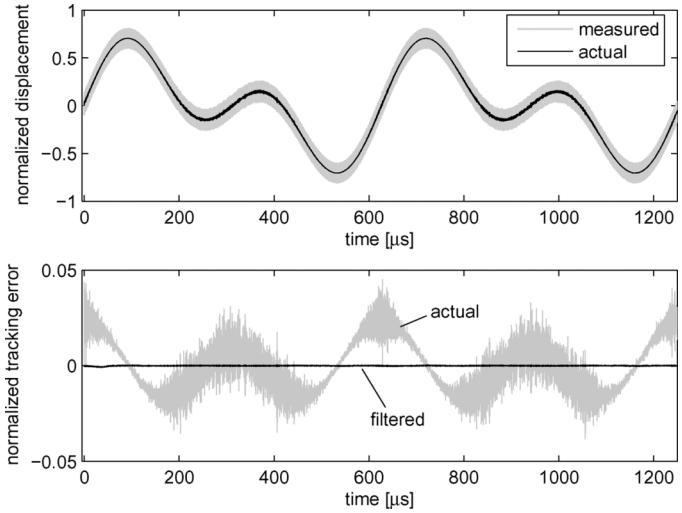

Fig. 12. Tracking performance in presence of measurement noise with $n_a = 0.1$.

Both full-state feedback and output feedback schemes have been developed, with guaranteed asymptotic output tracking. Simulation results show that the proposed adaptive control is effective for both set point regulation and trajectory tracking tasks. It can be seen from the control design that, in the adaptive setting, the output feedback treatment, which required the implementation of additional filters, became much more involved as compared to the full-state feedback case. If velocity measurements can be realized, then full-state feedback control can be implemented with relative ease.

REFERENCES

[1] P. B. Chu and S. J. Pister, "Analysis of closed-loop control of parallel-plate electrostatic microgrippers," in *Proc. IEEE Int. Conf. Robot. Autom.*, San Diego, CA, May 1994, pp. 820–825.

[2] J. L. Seeger and S. B. Crary, "Stabilization of electrostatically actuated mechanical devices," in *Proc. 9th Int. Conf. Solid-State Sensors Actuators (Transducers)*, Chicago, IL, Jun. 1997, pp. 1133–1136.

[3] E. K. Chan and R. W. Dutton, "Electrostatic micromechanical actuator with extended range of travel," *J. Microelectromech. Syst.*, vol. 9, no. 3, pp. 321–328, 2000.

[4] R. Nadal-Guardia, A. Dehé, R. Aigner, and L. M. Castañer, "Current drive methods to extend the range of travel of electrostatic microactuators beyond the voltage pull-in point," *J. Microelectromech. Syst.*, vol. 11, no. 3, pp. 255–263, 2002.

[5] J. Seeger and B. Boser, "Charge control of parallel-plate, electrostatic actuators and the tip-in instability," *J. Microelectromech. Syst.*, vol. 12, no. 5, pp. 656–671, 2003.

[6] G. Zhu, J. Lévine, and L. Praly, "Improving the performance of an electrostatically actuated MEMs by nonlinear control: Some advances and comparisons," in *Proc. 44th IEEE Conf. Dec. Control*, Seville, Spain, Dec. 2005, pp. 7534–7539.

[7] D. H. S. Maithripala, J. M. Berg, and W. P. Dayawansa, "Control of an electrostatic microelectromechanical system using static and dynamic output feedback," *J. Dyn. Syst., Meas., Control*, vol. 127, pp. 443–450, 2005.

[8] D. H. S. Maithripala, B. D. Kawade, J. M. Berg, and W. P. Dayawansa, "A general modelling and control framework for electrostatically actuated mechanical systems," *Int. J. Robust Nonlinear Control*, vol. 15, pp. 839–857, 2005.

[9] K. Nonaka, T. Sugimoto, J. Baillieul, and M. Horenstein, "Bi-directional extension of the travel range of electrostatic actuators by open loop periodically switched oscillatory control," in *Proc. 43rd IEEE Conf. Dec. Control*, Bahamas, Dec. 2004, pp. 1964–1969.

[10] T. Sugimoto, K. Nonaka, and M. N. Horenstein, "Bidirectional electrostatic actuator operated with charge control," *J. Microelectromech. Syst.*, vol. 14, no. 4, pp. 718–724, 2005.

[11] B. Borovic, A. Q. Liu, D. Popa, H. Cai, and F. L. Lewis, "Open-loop versus closed-loop control of MEMs devices: Choices and issues," *J. Micromech. Microeng.*, vol. 15, pp. 1917–1924, 2005.

[12] K. S. Narendra and A. M. Annaswamy, *Stable Adaptive Systems*. Englewood Cliffs, NJ: Prentice-Hall, 1989.

[13] J. E. Slotine and W. Li, *Applied Nonlinear Control*. Englewood Cliffs, NJ: Prentice-Hall, 1991.

[14] P. A. Ioannou and J. Sun, *Robust Adaptive Control*. Englewood Cliffs, NJ: Prentice-Hall, 1995.

[15] D. G. Taylor, P. V. Kokotovic, R. Marino, and I. Kanellakopoulos, "Adaptive regulation of nonlinear systems with unmodeled dynamics," *IEEE Trans. Autom. Control*, vol. 34, no. 4, pp. 405–412, Apr. 1989.

[16] I. Kanellakopoulos, P. V. Kokotovic, and R. Marino, "An extended direct scheme for robust adaptive nonlinear control," *Automatica*, vol. 27, pp. 247–255, 1991.

[17] S. S. Sastry and A. Isidori, "Adaptive control of linearizable systems," *IEEE Trans. Autom. Control*, vol. 34, no. 11, pp. 1123–1231, Nov. 1989.

[18] M. Krstic, I. Kanellakopoulos, and P. V. Kokotovic, *Nonlinear and Adaptive Control Design*. New York: Wiley, 1995.

[19] A. Shkel, R. Horowitz, A. Seshia, S. Park, and R. Howe, "Dynamics and control of micromachined gyroscopes," in *Proc. Amer. Control Conf.*, San Diego, CA, Jun. 1999, pp. 2119–2124.

[20] R. Leland, "Adaptive tuning for vibrational gyroscopes," in *Proc. 40th IEEE Conf. Dec. Control*, Orlando, Florida, Dec. 2001, pp. 3447–3452.

[21] S. Park and R. Horowitz, "Adaptive control for the conventional mode of operation of MEMs gyroscopes," *J. Microelectromech. Syst.*, vol. 12, no. 1, pp. 101–108, 2003.

[22] D. Piyabongkarn, Y. Sun, R. Rajamani, A. Sezen, and B. J. Nelson, "Travel range extension of a MEMs electrostatic microactuator," *IEEE Trans. Control Syst. Technol.*, vol. 13, no. 1, pp. 138–145, Jan. 2005.

[23] S. S. Ge, C. C. Hang, T. H. Lee, and T. Zhang, *Stable Adaptive Neural Network Control*. Boston, MA: Kluwer, 2001.

[24] S. S. Ge, K. P. Tee, I. Vahhi, and E. H. Tay, "Tracking and vibration control of flexible robots using shape memory alloys," *IEEE/ASME Trans. Mechatronics*, vol. 11, no. 6, pp. 690–698, Dec. 2006.

[25] K. P. Tee, S. S. Ge, and E. H. Tay, "Adaptive control of a class of uncertain electrostatic microactuators," in *Proc. Amer. Control Conf.*, NY, Jul. 2007, pp. 3186–3191.

[26] K. B. Ngo, R. Mahony, and Z. P. Jiang, "Integrator backstepping using barrier functions for systems with multiple state constraints," in *Proc. 44th IEEE Conf. Dec. Control*, Seville, Spain, Dec. 2005, pp. 8306–8312.

[27] J. J. Blech, "On isothermal squeeze films," *J. Lubrication Technol.*, vol. 105, pp. 615–620, 1983.

[28] M. Andrews, I. Harris, and G. Turner, "A comparison of squeeze-film theory with measurements on a microstructure," *Sensors Actuators A*, vol. 36, pp. 79–87, 1993.

[29] W. Kuehnel, "Modelling of the mechanical behaviour of a differential capacitor acceleration sensor," *Sensors Actuators A*, vol. 48, pp. 101–108, 1995.

[30] S. Vemuri, G. Fedder, and T. Mukherjee, "Low-order squeeze film model for simulation of MEMS devices," in *Proc. 3rd Int. Conf. Model. Simulation Microsyst.*, San Diego, CA, Mar. 2000, pp. 205–208.
[31] J. B. Lee and C. Goldsmith, "Numerical simulations of novel constant-charge biasing method for capacitive RF MEMS switch," in *Proc. NanoTech Conf.: Model. Simulation Microsyst.*, San Francisco, CA, Feb. 2003, pp. 396–399.
[32] J. D. Williams, R. Yang, and W. Wang, "Numerical simulation and test of a UV-LIGA-fabricated electromagnetic micro-relay for power applications," *Sensors Actuators A*, vol. 120, pp. 154–162, 2005.
[33] S. D. Senturia, *Microsystem Design*. Norwell, MA: Kluwer, 2001.
[34] M. Hoffmann, D. Nüsse, and E. Voges, "Electrostatic parallel-plate actuators with large deflections for use in optical moving-fibre switches," *J. Micromech. Microeng.*, vol. 11, pp. 323–328, 2001.
[35] D. A. Horsley, N. Wongkomet, R. Horowitz, and A. P. Pisano, "Precision positioning using a microfabricated electrostatic actuator," *IEEE Trans. Magn.*, vol. 35, no. 2, pp. 993–999, Feb. 1999.

Keng Peng Tee (S'04–M'08) received the B.Eng. and M.Eng. degrees both in mechanical engineering from the National University of Singapore, Singapore, in 2001 and 2003, respectively, where he is currently pursuing the Ph.D. degree in electrical and computer engineering.

In 2008, he became a Research Engineer with the Institute for Infocomm Research, Agency for Science, Research and Technology (A*STAR).

Dr. Tee was a recipient of the A*STAR Graduate Scholarship. His current research interests include intelligent/adaptive control theory and applications, robotics, and motor control.

Shuzhi Sam Ge (S'90–M'92–SM'99–F'06) received the B.Sc. degree from Beijing University of Aeronautics and Astronautics, Beijing, China, in 1986, and the Ph.D. degree and DIC from Imperial College, London, U.K., in 1993.

He is founding Director of the Social Robotics Lab, Interactive Digital Media Institute, and a Professor with the Department of Electrical and Computer Engineering, the National University of Singapore, Singapore. He has (co)-authored three books *Adaptive Neural Network Control of Robotic Manipulators* (World Scientific, 1998), *Stable Adaptive Neural Network Control*, (Kluwer, 2001) and *Switched Linear Systems: Control and Design* (Springer-Verlag, 2005); and edited the book *Autonomous Mobile Robots: Sensing, Control, Decision Making and Applications* (Taylor & Francis, 2006), and over 300 international journal and conference papers.

Dr. Ge is the founding Editor-in-Chief of *International Journal of Social Robotics* (Springer). He has served/been serving as an Associate Editor for a number of flagship journals including IEEE TRANSACTIONS ON AUTOMATIC CONTROL, IEEE TRANSACTIONS ON CONTROL SYSTEMS TECHNOLOGY, IEEE TRANSACTIONS ON NEURAL NETWORKS, and *Automatica*. He has been serving as Chair of Technical Committee on Intelligent Control, IEEE Control Systems Society since 2005, and an elected member of Board of Governors, IEEE Control Systems Society, 2007–2009.

He was the recipient of Changjiang Guest Professor, Ministry of Education, China, 2008; Outstanding Overseas Young Research Award, National Science Foundation, China, 2004; Inaugural Temasek Young Investigator Award, Singapore, 2002; Outstanding Young Researcher Award, National University of Singapore, 2001. He provides technical consultancy to industrial and government agencies. His current research interests include social robotics, multimedia fusion, adaptive control, intelligent systems and artificial intelligence.

Francis Eng Hock Tay is an Associate Professor with the Mechanical Engineering Department, National University of Singapore, Singapore. He is an active researcher in microsystems and some of his current research interests include biochip, wearable systems, and microfluidics. He is concurrently a Group Leader with the Medical Devices Group, Institute of Bioengineering and Nanotechnology. He has also been a Technical Manager of the Micro and Nano Systems Cluster, Institute of Materials Research and Engineering.